Chapter 12

Cardiac Imaging

Case 12.1: Coronary Calcium Screening

Clinical Information

A 59-year-old man with a history of hypertension and increased cholesterol level undergoing screening for coronary calcium.

Postprocessing Techniques Used and Approach

Axial data set is reconstructed at 3 mm and evaluated on the workstation (Table 12.1 and Figures 12.1.1 and 12.1.2). Foci of calcification in the coronary arteries are identified and circled to assign them to the appropriate artery. The computer performs automatic measurement of calcium score, and an automated but personalized report is generated (Table 12.2).

Diagnosis

Extensive coronary calcification.

Teaching Points

Coronary artery disease (CAD) remains the leading cause of death in the Western world. Unfortunately, death may be the initial event for patients with CAD. Screening for CAD is therefore of significant importance. Coronary calcium scoring has been used and researched for many years now. It started with electron beam CT (EBCT) but is now most often performed with MDCT scanners. With MDCT, patients are scanned with prospective ECG triggering using a partial scanner rotation to achieve improved temporal resolution. Reconstructions are relatively thick (2 mm to 3 mm) depending on the scanner, and are not suitable for 3D reconstruction.

The equivalence of calcium measurements obtained with MDCT and EBCT has been investigated. Most studies have shown good correlation between the two techniques. It has been argued that databases developed with EBCT studies on age- and sex-based calcium-score

Table 12.1. Scan Acquisition Parameters for Case 12.1, Coronary Calcium Screening

Slice No. and Thickness	16 × 1.0 mm
Coverage	Heart
Helical Pitch	Axial sequence with prospective gating
Rotation Speed	0.32 sec (partial scan)
Dose Parameters	120 kVp, 160 mAs
Contrast Dose	None

percentiles and risk profiles should not be applied to calcium scores obtained with MDCT scanners. This assertion is hard to justify given the close correlation of MDCT and EBCT for measuring the same physical entity—calcified tissue in the wall of the coronary arteries.

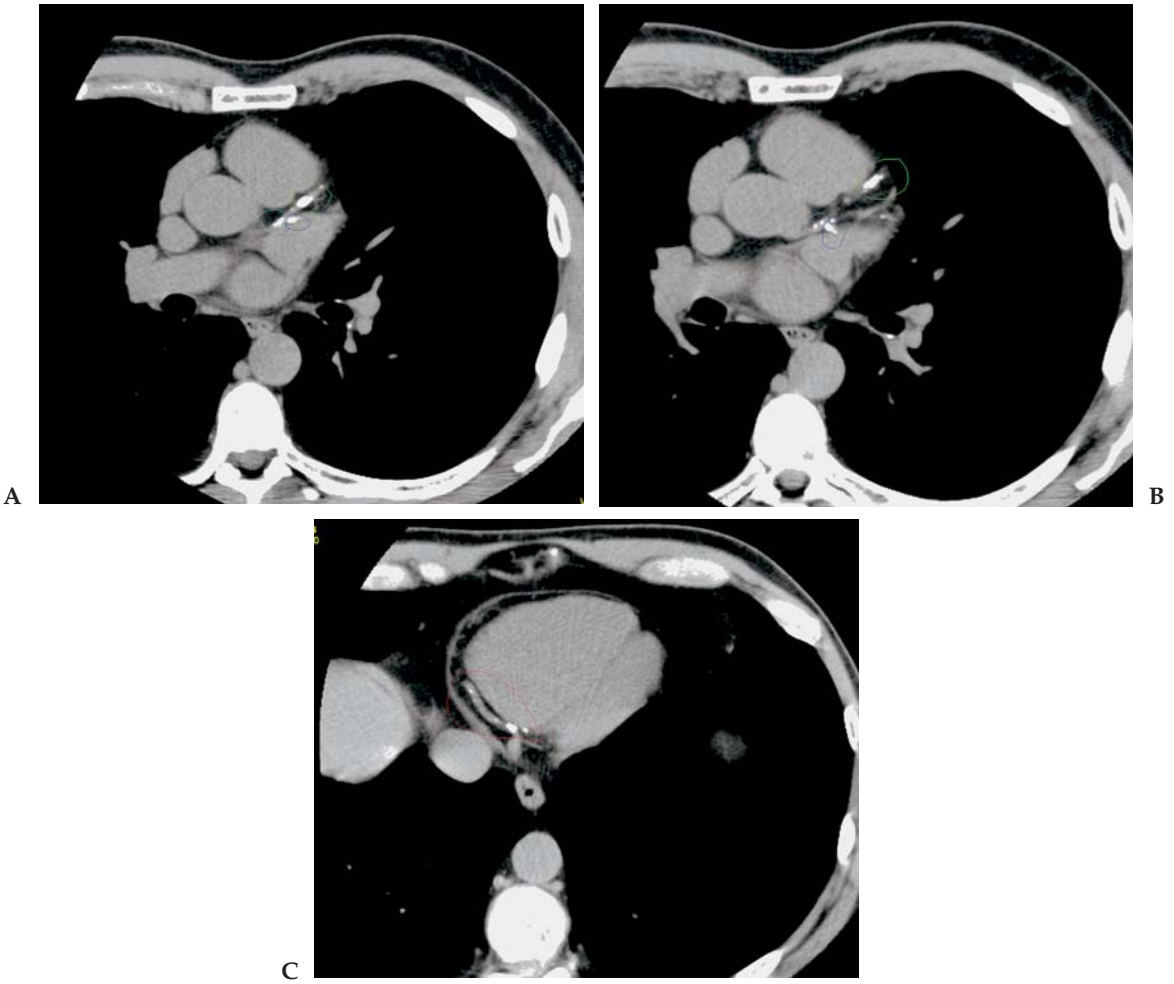

Figure 12.1.1. (A–C) Axial prospective gated images from a calcium scoring study. Calcific plaque is circled and assigned to the appropriate coronary artery. A sample of the extensive calcification in this patient is shown on these three images. Left main = turquoise, LAD = green, circumflex = blue, RCA = red.

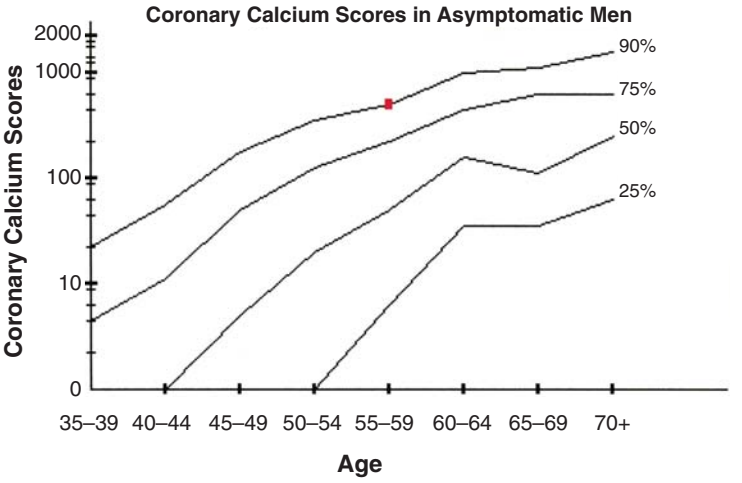

Figure 12.1.2. Curve demonstrating the patient's total calcium score plotted against age- and sex-matched controls.

One problem that is well recognized, however, is the significant interscan, interobserver, and intraobserver variability associated with calcium scoring. This limits the utility of the test to follow patients and assess responses to therapy. Some sites will routinely perform two acquisitions back-to-back on a patient and average the score to try to limit this variability.

The identification of coronary arterial calcification signifies the presence of atherosclerosis. Computed tomography is a very effective test to detect calcification and, therefore, coronary atherosclerosis. Currently, there is a lack of good prospective data to clearly show the utility of coronary calcium as a screening tool, but many studies are in progress. Current consensus from the American College of Cardiology/American Heart Association is summarized as follows:

1. A negative CT test makes the presence of atherosclerotic plaque, including unstable plaque, very unlikely.

Table 12.2. Summary Report of the Calcium Score by Artery With Total Score Using Both the Agatston and Volume Measurement Techniques

Region	Volume (mm^3)	Calcium Score (Agatston)
Left Main	37	21
Right Coronary Artery	159	172
Left Anterior Descending	152	187
Circumflex	72	83
Posterior Descending Artery	0	0
Total	420	463

2. A negative test is highly unlikely in the presence of significant luminal obstructive disease.
3. Negative tests occur in the majority of patients who have angiographically normal coronary arteries.
4. A negative test may be consistent with a low risk of a cardiovascular event in the next 2 years to 5 years.
5. A positive CT confirms the presence of coronary atherosclerotic plaque.
6. The greater the amount of calcium, the greater the likelihood of occlusive CAD, but there is not a one-to-one relationship, and findings may not be site specific.
7. The total amount of calcium correlates best with the total amount of atherosclerotic plaque, although the true "plaque burden" is underestimated.
8. A high calcium score may be consistent with moderate-to-high risk of a cardiovascular event within the next two years to five years.

A major criticism of calcium scoring has been that it does not show soft plaque, which is potentially more dangerous. Currently it is possible to perform a comprehensive cardiac examination combining coronary calcium scoring with coronary CTA. The combination of these two tests will show soft and hard plaque, measure stenosis, and quantify calcium burden. As 16-, 32-, and 64-detector scanners proliferate, this test will become widely available and may change how patients are screened.

Case 12.2: Coronary Artery CTA (Four Patients)

Clinical Information

Scans from four different currently asymptomatic patients aged from 53 years to 69 years who underwent screening for coronary artery disease.

Postprocessing Techniques Used and Approach

Images are reconstructed at multiple phases of the R-R interval using retrospective gating (Table 12.3 and Figures 12.2.1 through 12.2.4). The

Table 12.3. Scan Acquisition Parameters for Case 12.2, Coronary Artery CTA

Slice No. and Thickness	**16 × 0.5 mm**
Coverage	**Heart**
Helical Pitch	**0.25:1–0.3:1 (retrospective gating)**
Rotation Speed	**0.4 sec or 0.5 sec**
Dose Parameters	**120 kVp–135 kVp, 84 mAs–121 mAs**
Contrast Dose	**125 mL Omnipaque 350**
Injection Rate	**4 mL/sec**
Bolus Timing Method	**Bolus triggering on the ascending aorta**

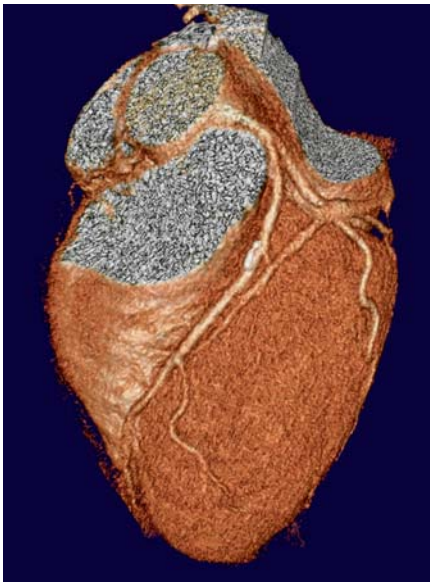

A

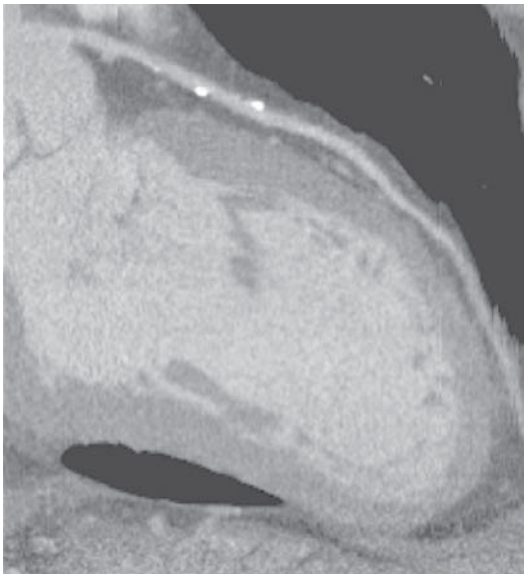

B

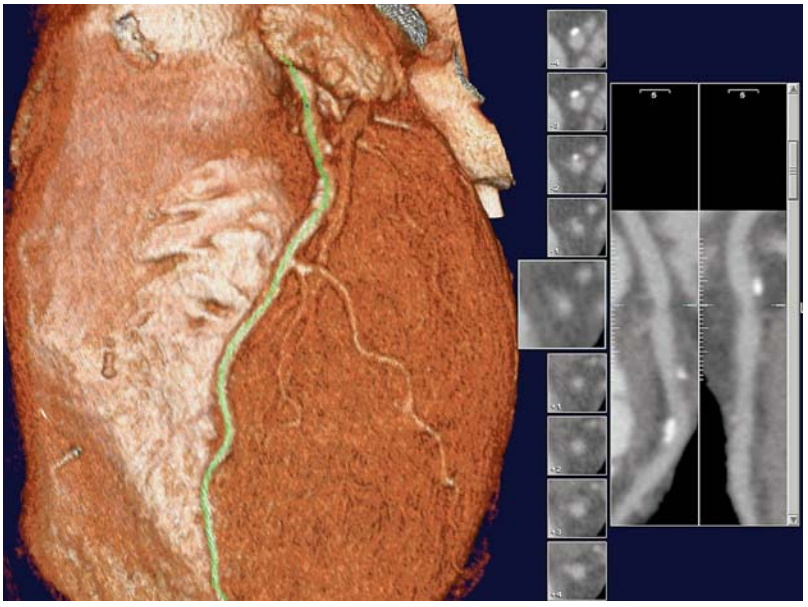

A

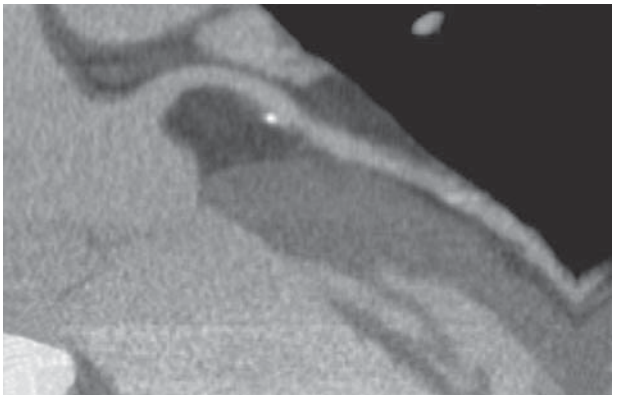

B

Figure 12.2.2. (A and B) Patient 2: Vessel-tracking software is used to generate a centerline path through the LAD and produce curved reconstructions with additional short axis views. Standard CPR is also shown. The proximal LAD contains multiple foci of both soft and calcified plaque. Luminal narrowing of approximately 30% is present.

Figure 12.2.3. (A–C) Patient 3: Volume-rendered image of the LAD demonstrates dense calcified plaque, which essentially obscures the underlying vessel. Curved planar reconstructions shows extensive soft and calcific plaque, which appears to cause stenosis of greater than 90% in areas. Axial 0.5-mm image shows that there is some motion artifact, which can magnify the calcium blooming artifact and cause overestimation of vessel stenosis. Catheter angiogram in this patient showed the luminal narrowing in the LAD was no more than 50% to 60%.

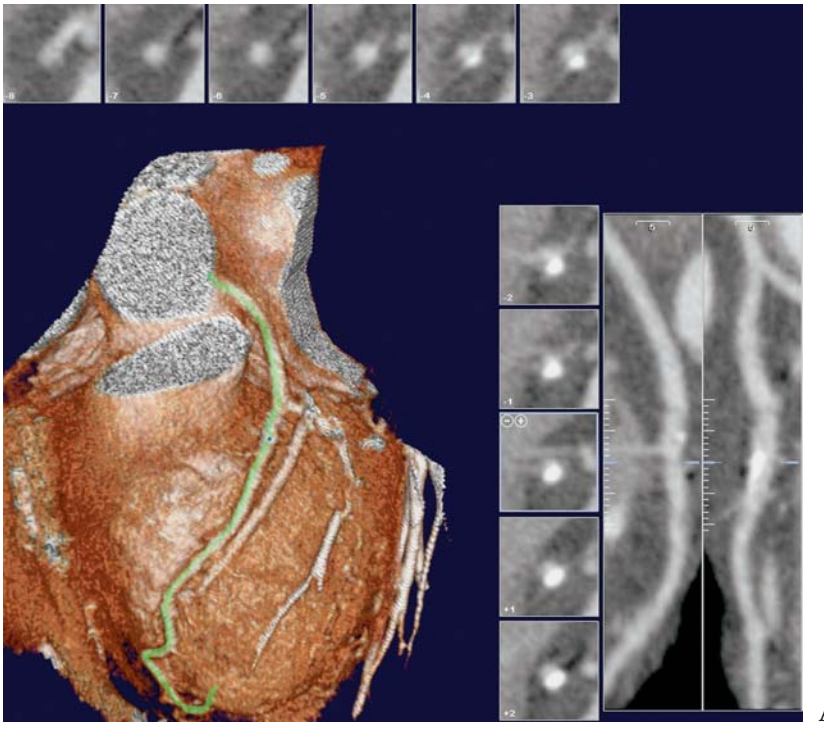

A

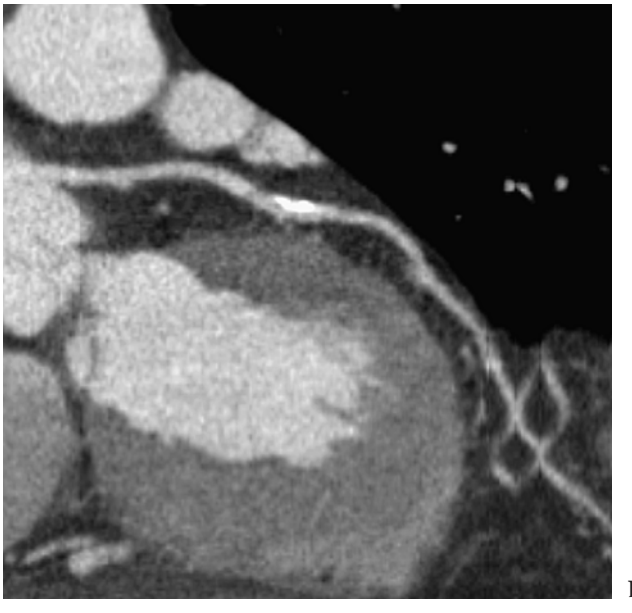

B

Figure 12.2.4. (A and B) Patient 4: vessel-tracking view and CPR through the LAD. There is an eccentric calcified plaque, which causes a stenosis of approximately 70%. This is best measured on the axial short axis views. Findings were confirmed by cardiac catheterization.

best quality data set with the least motion is selected for evaluation. For the left anterior descending (LAD) and circumflex arteries this is generally in diastole at 70% or 80% R-R interval. For the right coronary artery (RCA) this is more variable, between 40% and 70% R-R interval. Volume-rendered images are reviewed to demonstrate the morphology of the involved arteries. Manual segmentation is performed from the 3D images to remove the diaphragm and overlying vascular structures that limit visualization of the vessels. Curved planar reconstructions are generated using automated software to visualize the vessel lumen and plaque deposits.

Diagnosis

Patient 1: mild calcific plaque without significant stenosis. Patient 2: moderate soft and calcific plaque with areas of luminal narrowing measuring less than 40%. Patient 3: dense calcified plaque present. Stenosis on CT was estimated at 90%, however a catheter angiogram was performed, which showed no lesion greater than 50% to 60%. Patient 4: 70% stenosis of the LAD secondary to an eccentric calcified plaque. This was confirmed by angiogram.

Teaching Points

Coronary artery disease remains the leading cause of death and disability in the Western world for both men and women. The financial cost of the disease is staggering. Although many patients have symptoms of ischemia or myocardial infarction, for many other patients their first event results in sudden death. Currently catheter coronary angiography is the gold standard for diagnosis of CAD. This test is expensive and invasive, however, and clearly not suitable for screening patients. It is performed frequently as a second-line test for diagnostic and therapeutic purposes. However, only one third of all conventional coronary angiographic examinations in the United States are performed in conjunction with an interventional procedure, while the rest are performed only for diagnostic purposes. Many of these examinations could be avoided if an accurate and noninvasive test were available.

Coronary artery CTA is a very exciting and rapidly progressing field. The initial research with 4-slice scanners yielded results that were less than ideal. These scanners were limited by long acquisition times (breath holds of more than 30 sec) and low spatial resolution. Early results with 16-detector scanners have been more promising. For stenosis of 50% or greater, detection accuracy has been shown to approach 90%. A normal CTA examination has also been found to have a very high negative predictive value of a normal coronary CTA (97% with 16-detector scanners). This high negative predictive value demonstrates the utility of a noninvasive CTA as a reliable test to exclude CAD in the large population of patients with equivocal clinical presentation and findings. Many of these patients will end up with a costly workup that may include cardiac catheterization.

Another very exciting aspect of coronary CTA is the potential ability to perform plaque characterization. Currently, the only other diagnostic test that has this ability is intravascular ultrasound. Studies have shown that the plaque composition is tied to its risk of rupture and sudden death or severe ischemia. Lipid-rich noncalcified plaques are most prone to spontaneous rupture and are known as "vulnerable plaque." Calcified and fibrous plaques are more stable and chronic and less likely to rupture. Excessive vessel calcification currently is a limitation of coronary CTA. The blooming effect of the calcium may cause overestimation of stenosis, particularly if motion is present. For this reason many sites will screen patients first with a coronary calcium study, and if extensive calcium is present, will forego the CTA.

The obvious benefit of accurate noninvasive identification of vulnerable plaque is that cardiologists can intervene preemptively before an acute coronary event, either by invasive means such as angioplasty and stenting, or by pharmacologic means such as statin therapy. This is an area that will require additional research in the future.

The future holds considerable promise for cardiac CTA, particularly with 64-detector scanners. These scanners can decrease acquisition time to less than 10 sec with spatial resolution of 0.5 mm to 0.625 mm. The shorter breath hold improves patient cooperation and decreases heart rate variability that occurs frequently in longer breath holds. This produces a better quality data set. The main problem for cardiac CTA is temporal resolution. Additional improvements in gantry rotation time will be difficult because of the very high g-forces involved. Therefore, improved temporal resolution will primarily require software improvements using adaptive segmented reconstruction or other new techniques.

Case 12.3: Bypass Graft Evaluation

Clinical Information

A 70-year-old man with prior two-vessel bypass, undergoing evaluation for bypass graft patency.

Postprocessing Techniques Used and Approach

Images are reconstructed using retrospective gating at 10% R-R intervals from 10% to 90% (Table 12.4 and Figures 12.3.1 and 12.3.2). Volume-rendered images are reviewed to demonstrate the morphology of the grafts. Some manual segmentation is performed from the 3D images to remove overlying vascular structures that limit visualization of the grafts. Curved planar reconstructions are generated using automated software.

Diagnosis

Patent left internal mammary artery (IMA) to left anterior descending artery graft and patent saphenous vein graft to the RCA.

Table 12.4. Scan Acquisition Parameters for Case 12.3, Bypass Graft Evaluation

Slice No. and Thickness	**16 × 1.0 mm**
Coverage	**Lung apex through heart**
Helical Pitch	**0.25:1 (retrospective gating)**
Rotation Speed	**0.4 sec**
Dose Parameters	**135 kVp, 96 mAs**
Contrast Dose	**125 mL Omnipaque 350**
Injection Rate	**4 mL/sec**
Bolus Timing Method	**Bolus triggering on the ascending aorta**

Teaching Points

Coronary artery bypass surgery with use of either venous or internal mammary artery bypass grafts is an established treatment for symptomatic multivessel coronary artery disease. One of the most important variables that determines the successful clinical outcome of coronary artery bypass graft placement is the short- and long-term patency rate of the grafts. For venous coronary artery bypass grafts, an occlusion rate of 12% to 20% has been reported within the first year after surgery.

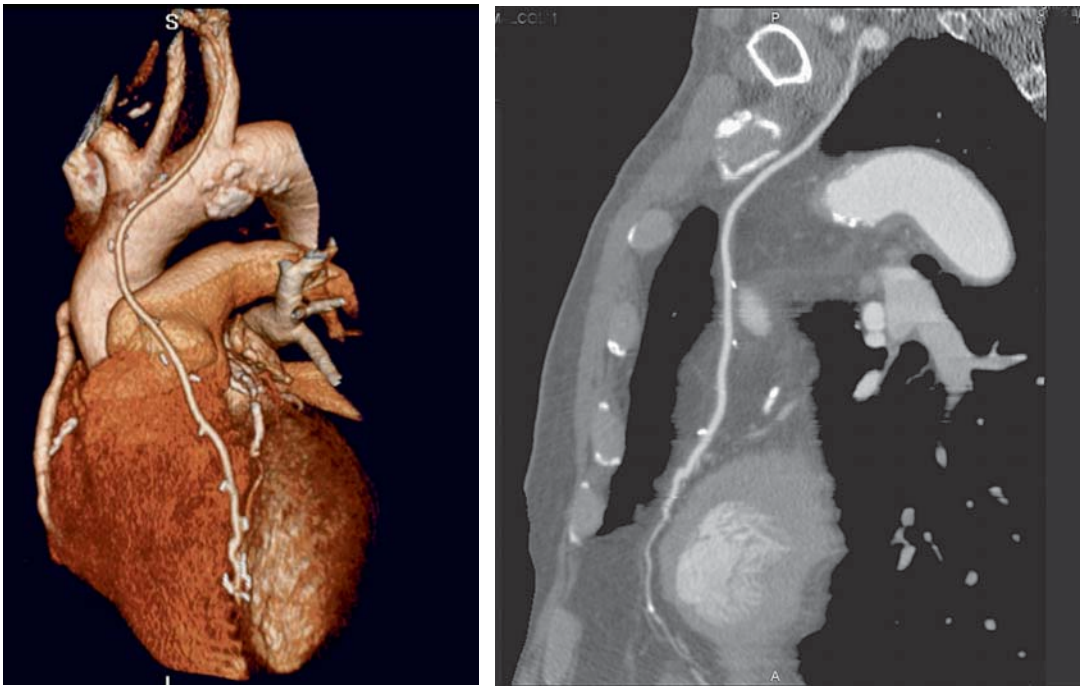

A B

Figure 12.3.1. (A and B) Volume-rendered image demonstrates the left internal mammary artery (LIMA) graft extending from the left subclavian artery to the LAD. The CPR demonstrates patency of the graft without significant stenosis and patency of the LAD distal to the anastomosis. (Courtesy of Dr. Ruben Sebben, Dr. Jones & Partners Medical Imaging, South Australia.)

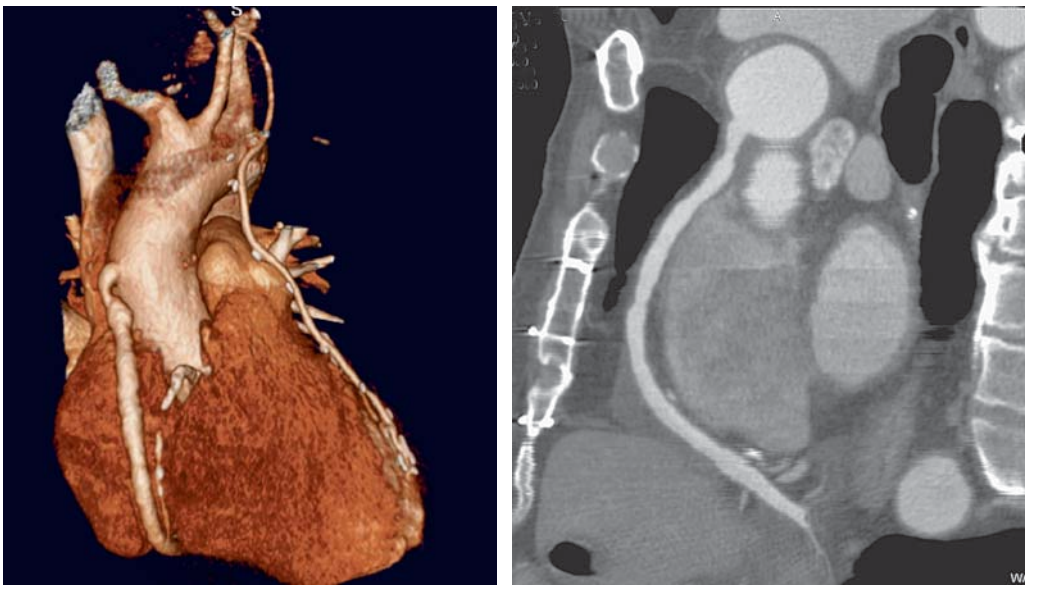

Figure 12.3.2. (A and B) Volume-rendered and curved images show patency of the right coronary artery saphenous vein graft. (Courtesy of Dr. Ruben Sebben, Dr. Jones & Partners Medical Imaging, South Australia.)

After 5 years postsurgery, the occlusion rate is 4% per year. For IMA bypass grafts, the occlusion rate is approximately 10% after 10 years postimplantation.

Currently cardiac catheterization remains the standard procedure to evaluate bypass grafts for patency and stenosis. However, because of the invasive nature of that examination it is generally not performed for evaluation of grafts unless patients are significantly symptomatic. Multidetector CT now offers a noninvasive test to accurately determine graft patency and morphology. Computed tomography can be used for surveillance of grafts following surgery, and it is also very helpful to a cardiac surgeon for demonstrating the precise location of the bypass grafts prior to a redo coronary bypass operation.

One significant danger of reoperation is injury to an existing graft that can occur during the sternotomy. There is a reported injury rate of 5.3% to patent left internal mammary artery (LIMA) grafts during re-operative bypass procedures, and the risk for right internal mammary artery (RIMA) grafts is even higher. Computed tomography can demonstrate grafts in unusual locations and warn the surgeon of a bypass graft immediately adjacent or adhesed to the sternum. Other graft complications, such as formation of a pseudoaneurysm, can also be detected.

Table 12.5. Scan Acquisition Parameters for Case 12.4, Aberrant Right Coronary Artery

Slice No. and Thickness	**16 × 0.5 mm**
Coverage	**Through heart**
Helical Pitch	**0.25:1 (retrospective gating)**
Rotation Speed	**0.5 sec**
Dose Parameters	**135 kVp, 180 mAs**
Contrast Dose	**150 mL Omnipaque 350**
Injection Rate	**4 mL/sec**
Bolus Timing Method	**Bolus triggering on the ascending aorta**

Case 12.4: Aberrant Right Coronary Artery

Clinical Information

A 40-year-old weight lifter who notices chest pain during strenuous workouts.

Postprocessing Techniques Used and Approach

Images are reconstructed using retrospective gating at 10% R-R intervals from 10% to 90% (Table 12.5 and Figures 12.4.1 through 12.4.3). Volume-rendered images of the heart are used to show the coronary artery anatomy. Segmentation to remove the pulmonary artery is performed manually from 2D images. Coronal curved reformations are also generated with automated software.

Diagnosis

Aberrant origin of the right coronary artery, which arises on the left above the left coronary artery. The vessel then courses to the right between the aorta and pulmonary artery.

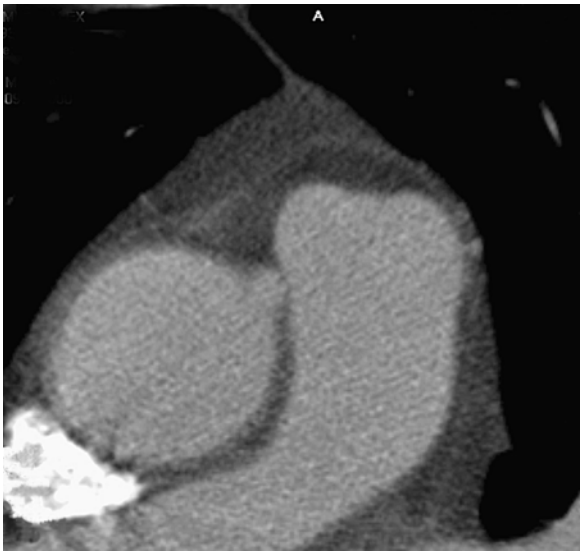

Figure 12.4.1. Axial image demonstrating the origin of the right coronary artery from the left side of the aorta adjacent to the main pulmonary artery.

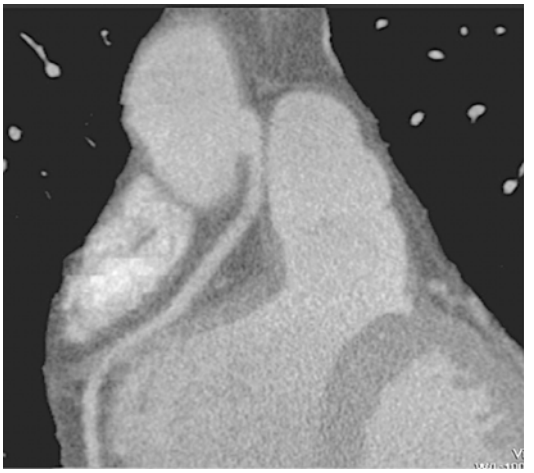

A

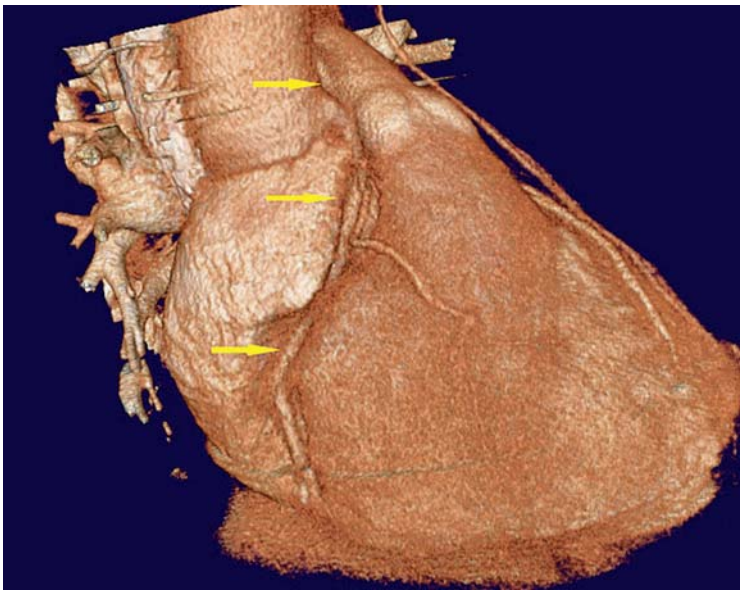

B

Figure 12.4.2. (A and B) Coronal curved planar reconstruction and VR image through the heart. The path of the RCA (arrows), which arises from the left side of the aorta and passes between the aorta and the main pulmonary artery before entering the atrioventricular groove, is clearly shown.

Teaching Points

Coronary artery anomalies are relatively common and have been reported in up to 2% of the population. Many anomalies are benign; however, certain anomalies can result in myocardial ischemia and death.

Coronary anomalies include abnormalities of coronary origin and are highly variable. Typical anomalies include origin of a coronary artery from the pulmonary trunk, left or right ventricle, or high on the aorta or great vessels. Another common anomaly is origination of the

Figure 12.4.3. Segmented VR image with the pulmonary artery cut away. The relationship between the origin of the right and left main coronary arteries is now seen.

coronary ostium from the opposite, facing coronary sinus, and cases of single coronary artery. Other patients may have abnormalities related to abnormal course, termination, or structure of the coronary artery. Examples include myocardial bridges, coronary fistulas, and congenital stenosis or atresia of a coronary artery.

In this patient with an aberrant right coronary artery that arises on the left above the normal coronary cusp and has an abnormal course, the main symptom was exercise-induced chest pain. Ischemia may result from compression of the coronary artery between the aorta and the pulmonary trunk. This can occur during periods of exercise when these vessels undergo vasodilatation.

In this case CTA provided excellent documentation of the origin and course of the aberrant coronary artery. The origin of the RCA in this case was relatively high, well above the left coronary cusp. Had the origin been lower, near the left cusp, the ischemia would likely be worse. In cases of significant compression, treatment is surgical. Either surgical reimplantation of the aberrant artery or bypass can be performed.

Case 12.5: Pulmonary Vein Evaluation

Clinical Information

A 67-year-old woman with atrial fibrillation undergoing evaluation for radiofrequency ablation.

Table 12.6. Scan Acquisition Parameters for Case 12.5, Pulmonary Vein Evaluation

Slice No. and Thickness	**16 × 0.5 mm**
Coverage	**Chest**
Helical Pitch	**0.25:1 (cardiac gated study)**
Rotation Speed	**0.4 sec**
Dose Parameters	**120 kVp, 250 mAs**
Contrast Dose	**125 mL Omnipaque 350**
Injection Rate	**4 mL/sec**
Bolus Timing Method	**Bolus triggering on ascending aorta**

Postprocessing Techniques Used and Approach

The examination was performed as a retrospective cardiac gated study with reconstruction of images at 80% of the R-R interval (Table 12.6 and Figures 12.5.1 through 12.5.4). Processing is performed on the workstation. Initial volume-rendered views of the atrium and pulmonary veins are obtained after manual segmentation to remove the spine and descending thoracic aorta. Coronal and axial thin- and thick-slab MIP images are reviewed to identify and measure the pulmonary veins and

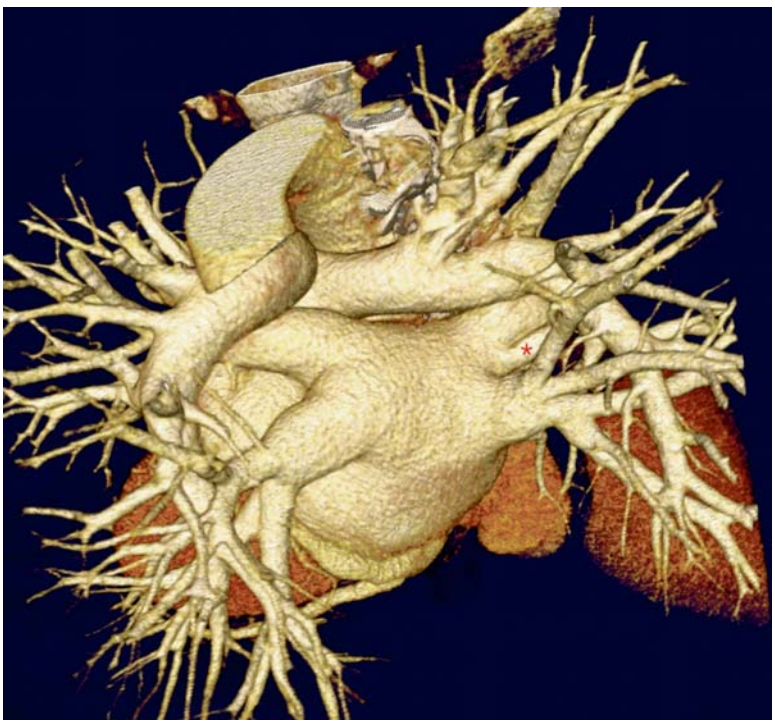

Figure 12.5.1. Volume-rendered image of the left atrium and pulmonary veins. The aorta and spine have been removed. Note the accessory pulmonary vein to the right middle lobe (*).

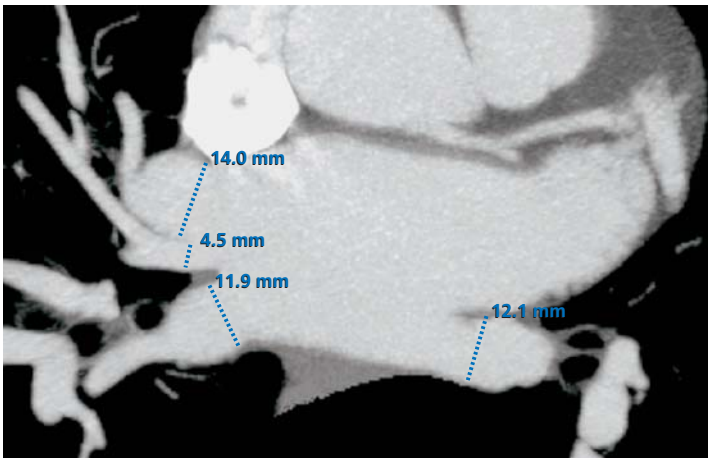

Figure 12.5.2. Axial MIP image demonstrating measurement of the right upper, middle, and lower veins, and the left lower vein. The atrial appendage is shown, but the left upper vein is not included on this image.

left atrium. Finally, endoluminal fly-through imaging is performed within the left atrium to visualize the pulmonary vein ostia. Three-dimensional markers arrows can be place on the 2D images to facilitate identification of the veins on the endoluminal images.

Diagnosis

Pulmonary vein mapping prior to radiofrequency ablation.

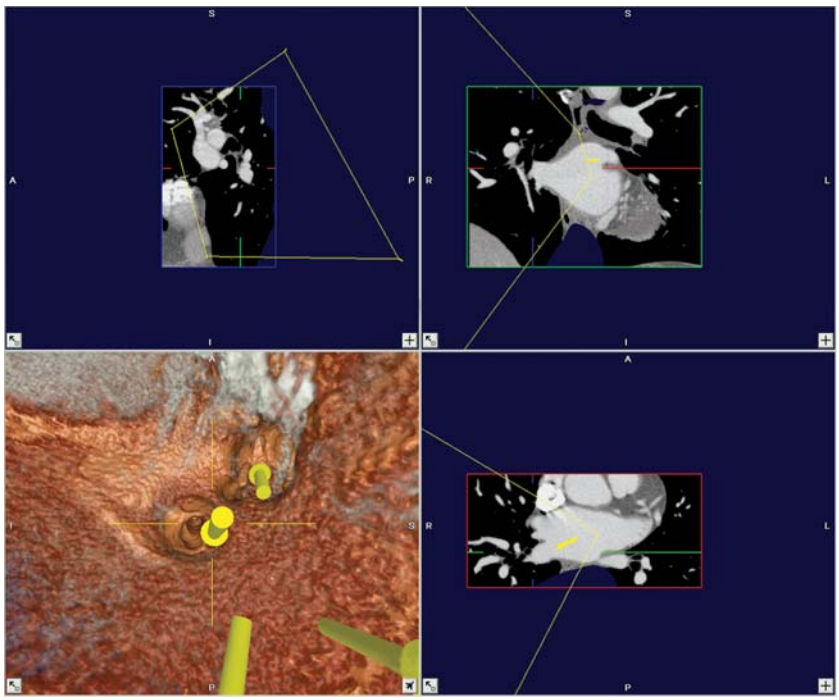

Figure 12.5.3. Navigation view showing localization of the right-sided pulmonary veins. The 3D marker arrows are seen.

Figure 12.5.4. Magnified view of the right pulmonary veins. The right, middle, and upper lobe veins have a conjoined origin.

Teaching Points

Atrial fibrillation (AF) is an important clinical problem with significant potential morbidity, particularly cerebrovascular accidents. Many patients can be adequately treated with medical therapy; however, some patients are refractory to medical management. Atrial fibrillation occurs when multiple ectopic electrical foci fire independently of the sinoatrial (SA) node. Instead of receiving one electrical signal, the atrioventricular (AV) node is bombarded by up to 300 discharges per minute.

The muscular sleeves of the pulmonary veins are a major source of ectopic electrical foci. Recently, it has been discovered that paroxysms of atrial fibrillation are initiated by trains of spontaneous activity originating from the pulmonary veins in 90% to 96% of patients, with almost half arising in the left superior pulmonary vein. Cardiologists are now performing radiofrequency catheter ablation (RFCA) to suppress these ectopic foci. The RFCA works by electrically isolating the conduction pathways through ablation of the distal pulmonary veins and posterior left atrium.

During RFCA, radiofrequency energy is preferably applied at the venoatrial junction of all the pulmonary veins to avoid stenoses and eliminate ostial remnants that may contribute to recurrent atrial fibrillation. Therefore, advance knowledge of how many pulmonary veins are present, and their ostial locations, is important to ensure that all the ostia are ablated. It is difficult and time-consuming to locate the ostia with conventional angiography at the time of ablation.

Since successful RFCA depends in part on good preprocedural mapping, MDCT can be used to evaluate the left atrium and pul-

monary veins. Evaluation should include discussion of size, number and location of pulmonary veins, description of anatomic variants, and the presence of ostial branches. Left atrial volume can also be measured, and thrombi in the atrium or atrial appendage must be excluded. Anatomy of the pulmonary veins is highly variable, with variations reported in 30% to 40%, including accessory veins (usually on the right) and conjoined veins (usually on the left). The distance from the ostium to the first major branch is also important.

Computed tomography of the atrium and pulmonary veins can be performed with either gated or nongated technique. Gating is generally preferred, as it will minimize motion artifacts, but in patients with very irregular heart rates it may not be possible and it is not suggested for ill patients who cannot hold their breath for the entire study. Also, gated studies increase radiation exposure.

Workstation evaluation should include segmentation with volume rendering to show the atrium and pulmonary veins; thin and thick slab MIP images to show anatomy, measure size of the venous ostia, and look for thrombi; and endoluminal images to demonstrate ostial branches and provide a map for the electrophysiologist.

Case 12.6: Atrial Myxoma

Clinical Information

A 57-year-old woman with a history of chest pain and dyspnea undergoing evaluation to rule out pulmonary embolus.

Postprocessing Techniques Used and Approach

Multiplanar axial, sagittal, and coronal images are reviewed (Table 12.7 and Figure 12.6.1).

Diagnosis

Myxoma of the left atrium.

Teaching Points

Although this was not a gated cardiac study, excellent visualization of the atria and ventricles is obtained routinely on nongated CTAs. The

Table 12.7. Scan Acquisition Parameters for Case 12.6, Atrial Myxoma

Slice No. and Thickness	**16 × 1.0 mm**
Coverage	**Through chest**
Helical Pitch	**1.25:1**
Rotation Speed	**0.5 sec**
Dose Parameters	**120 kVp, 200 mAs**
Contrast Dose	**125 mL Omnipaque 350**
Injection Rate	**3 mL/sec**
Bolus Timing Method	**Sure start on pulmonary artery**

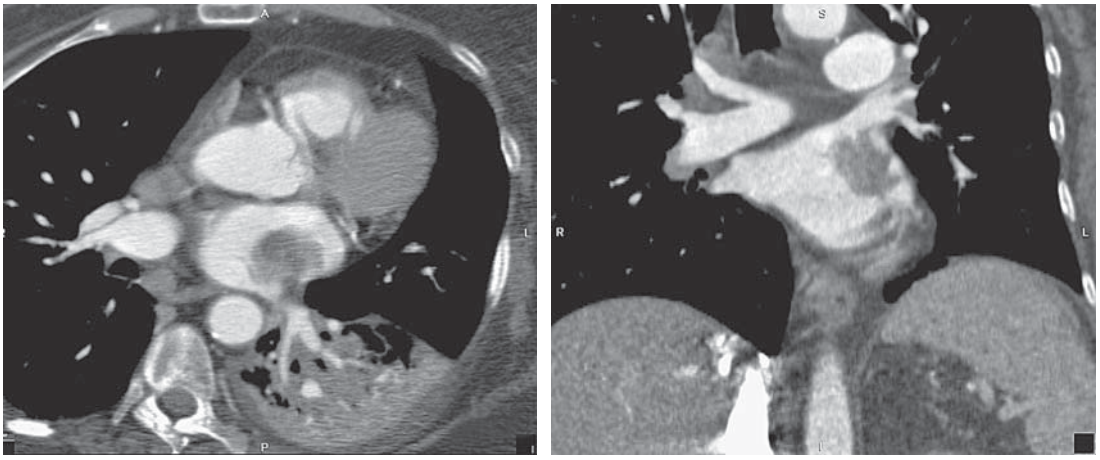

A B

Figure 12.6.1. (A and B) Axial and coronal 2-mm images focused on the heart show a polypoid mass with a stalk arising from the left atrium. Appearance is consistent with a left atrial myxoma.

atrial tumor was an unsuspected finding in this patient but was likely the cause of her symptoms.

Cardiac myxoma is a benign neoplasm that accounts for approximately one half of all primary cardiac tumors. Myxoma typically manifests as a polypoid, intracavitary atrial mass that arises from the interatrial septum. Left atrial involvement is four times more common than right atrial involvement, but myxoma may originate in any cardiac chamber. Most affected patients have at least one feature of a classically described triad that includes cardiac obstructive symptoms, constitutional symptoms, and embolic events.

Presenting complaints relate to tumor location, which predicts obstructive sequelae and influences embolic sites (pulmonary or systemic). Left atrial myxomas commonly cause mitral valve obstruction. Affected patients may have dyspnea and orthopnea from pulmonary venous hypertension. The pedunculated and prolapsing nature of these tumors allows for positional and intermittent mitral valve obstruction. Of patients in a large series with left atrial myxomas, 60% had symptoms related to mitral valve obstruction. Right atrial myxomas may obstruct the tricuspid valve and cause symptoms of right-sided heart failure, peripheral edema, passive hepatic congestion, and syncope. In this series, only 9% of patients with right atrial myxomas had signs and symptoms of tricuspid valve obstruction.

Constitutional symptoms of fever, malaise, weight loss, anemia, and elevated sedimentation rate have been reported and may be related to an autoimmune reaction initiated by the tumor. These symptoms can be seen in 25% to 30% of patients. Cardiac arrhythmias, atrial fibrillation, and atrial flutter reportedly occur in approximately 20% of patients with cardiac myxoma. Embolic phenomena are reported in approximately 35% of left-sided and 10% of right-sided myxomas.

Table 12.8. Scan Acquisition Parameters for Case 12.7, Coronary Stent Evaluation

Slice No. and Thickness	**16 × 0.5 mm**
Coverage	**Heart**
Helical Pitch	**0.25:1 (retrospective gating)**
Rotation Speed	**0.4 sec**
Dose Parameters	**135 kVp, 98 mAs–114 mAs**
Contrast Dose	**125 mL Omnipaque 350**
Injection Rate	**4 mL/sec**
Bolus Timing Method	**Bolus triggering on the ascending aorta**

Case 12.7: Coronary Stent Evaluation (Two Patients)

Clinical Information

Two patients undergoing evaluation of coronary stents for patency.

Postprocessing Techniques Used and Approach

Images are reconstructed at multiple phases of the R-R interval using retrospective gating (Table 12.8 and Figures 12.7.1 and 12.7.2). The best quality data set with the least motion is selected for evaluation. For the circumflex artery this was 80% R-R interval, and for the RCA, 50% R-R interval. Volume-rendered images are reviewed to demonstrate the morphology of the involved arteries and show the location of the stent. Manual segmentation is performed from the 3D images to remove the diaphragm and overlying vascular structures that limit visualization of the vessels. Curved planar reconstructions are generated using automated software to visualize the lumen inside the stent.

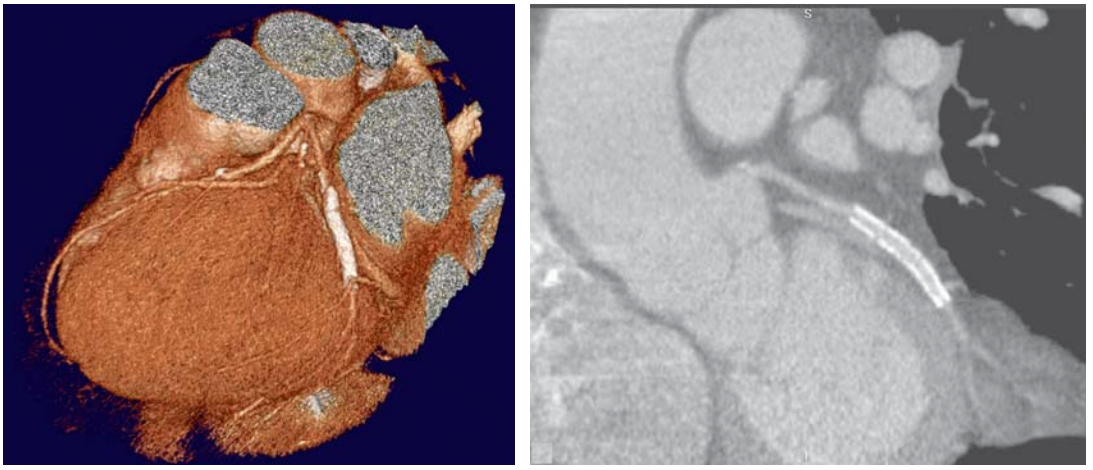

A B

Figure 12.7.1. (A and B) Patient 1: three-dimensional volume-rendered and curved planar reconstructions of a stent in the circumflex coronary artery. Stent patency is confirmed.

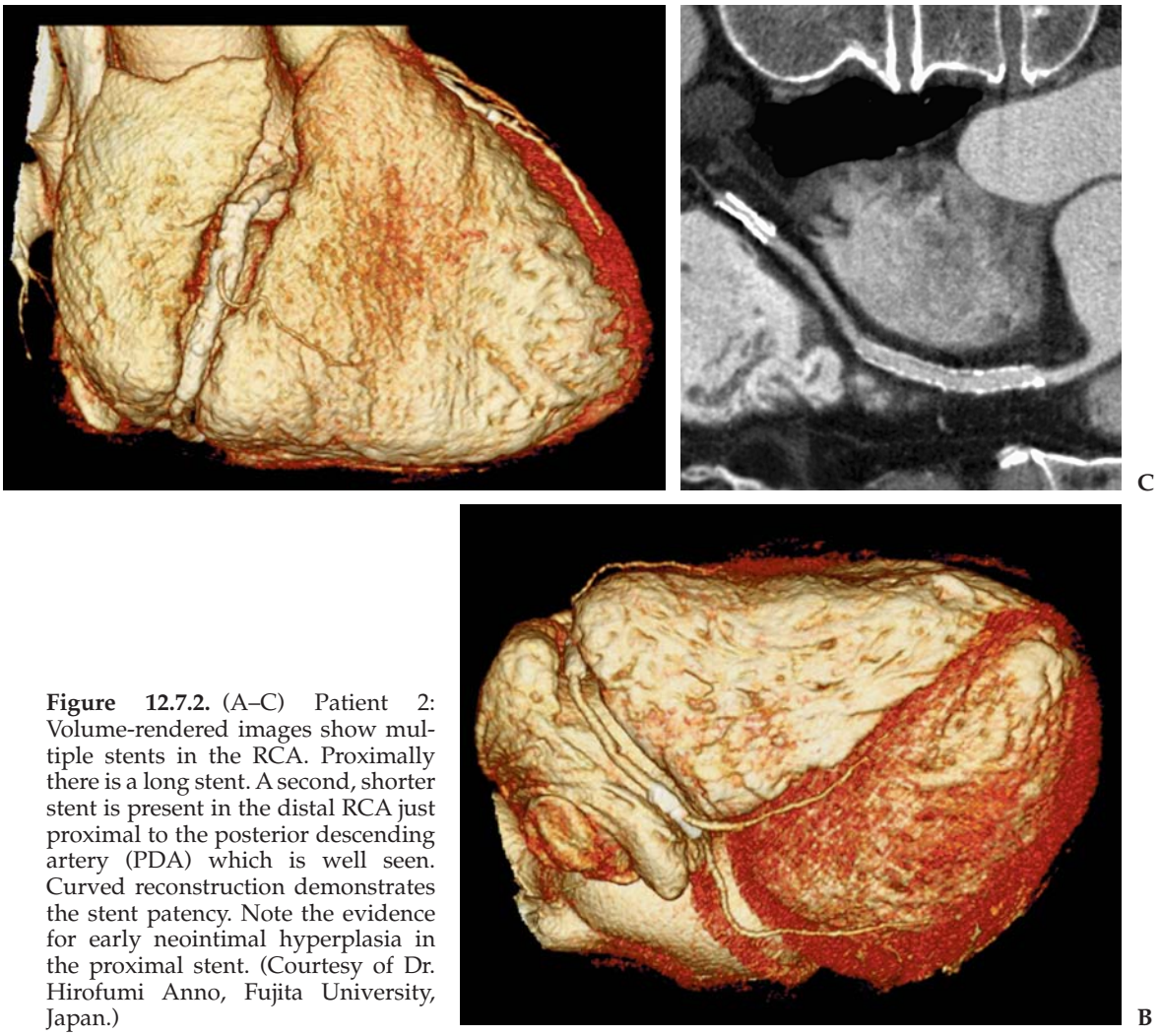

Figure 12.7.2. (A–C) Patient 2: Volume-rendered images show multiple stents in the RCA. Proximally there is a long stent. A second, shorter stent is present in the distal RCA just proximal to the posterior descending artery (PDA) which is well seen. Curved reconstruction demonstrates the stent patency. Note the evidence for early neointimal hyperplasia in the proximal stent. (Courtesy of Dr. Hirofumi Anno, Fujita University, Japan.)

Diagnosis

Patient 1: patent stent in the circumflex artery. Patient 2: patent stents in the right coronary artery.

Teaching Points

Coronary artery stent placement has become the accepted standard of practice for the percutaneous treatment of coronary artery stenosis in both acute and chronic coronary artery disease. Coronary artery stent placement reduces early complications of percutaneous transluminal coronary angioplasty (PTCA), as well as restenosis rates, and thus improves the safety and efficacy of angioplasty. Although patency rates are much better for stented vessels compared with vessels treated by PTCA alone, neointimal hyperplasia remains a significant problem and

can lead to vessel occlusion. This risk has led to the routine use of invasive and costly coronary angiography for surveillance of stent patency and stenosis. There is therefore a clinical need for a less expensive and noninvasive test that can successfully evaluate coronary stents.

Early studies with 4-detector MDCT had mixed result for the evaluation of stents, but more recent studies with 16-detector scanners have shown good results for CT stent evaluation. Hong et al. was able to adequately evaluate 20 stents out of 26 stents in 19 patients. In 5 patients, 6 stents could not be adequately evaluated because of too much motion or gating failure.

One major difficulty of CT stent evaluation is partial volume averaging associated with the metal struts of the stent. These struts will also accentuate motion streak artifacts if present. It is therefore very important to use the highest spatial resolution possible (0.5 mm to 0.625 mm) for data acquisition. Multiple cardiac phases must also be reconstructed and carefully reviewed for the phase with the least motion for each involved artery. It has also been shown that reconstructing the images with a sharp kernel rather than a soft tissue kernel will improve visualization of the stent lumen, although the images will be noisier.

Selected Readings

Coronary Calcium Screening

1. Callister TQ, et al. Coronary artery calcium scores on electron beam computed tomography. JACC 1999;33(suppl):415A.
2. Carr JJ, et al. Evaluation of subsecond gated helical CT for quantification of coronary artery calcium and comparison with electron beam CT. Am J Roentgenol 2000;174:915–921.
3. Mayo Clinic Proceedings. Findings based on EBCT data. March 1999, Vol. 74.
4. Nieman K, Oudkerk M, Rensing BJ, et al. Coronary angiography with multi-slice computed tomography. Lancet 2001;357:599–603.
5. O'Malley PG, Taylor AJ, Gibbons RV, et al. Rationale and design of the Prospective Army Coronary Calcium (PACC) study: utility of electron beam computed tomography as a screening test for coronary artery disease and as an intervention for risk factor modification among young, asymptomatic, active-duty United States Army personnel. Am Heart J 1999;137:932–941.
6. O'Rourke R, Brundage B, Froelicher V, et al. American College of Cardiology/American Heart Association Expert Consensus document on electron-beam computed tomography for the diagnosis and prognosis of coronary artery disease. Circulation 2000;102:126–140.
7. Schoepf UJ, Becker CR, Ohnesorge BM, Yucel EK. CT of coronary artery disease. Radiology 2004;232:18–37.

Coronary Artery CTA

8. Achenbach S, Giesler T, Ropers D, et al. Detection of coronary artery stenoses by contrast-enhanced, retrospectively electrocardiographically-gated, multislice spiral computed tomography. Circulation 2001;103: 2535–2538.

9. Becker CR, Knez A, Ohnesorge B, Schoepf UJ, Reiser MF. Imaging of noncalcified coronary plaques using helical CT with retrospective ECG gating. Am J Roentgenol 2000;175:423–424.
10. Choi HS, Choi BW, Choe KO, et al. Pitfalls, artifacts, and remedies in multidetector row CT coronary angiography. Radiographics 2004;24:787–800.
11. Desjardins B, Kazerooni EA. ECG-gated cardiac CT. Am J Roentgenol 2004 Apr;182:993–1010.
12. Kopp A, Kuttner A, Heuschmid M, Schroder S, Ohnesorge B, Claussen C. Multidetector-row CT cardiac imaging with 4 and 16 slices for coronary CTA and imaging of atherosclerotic plaques. Eur Radiol 2002;12:S17–S24.
13. Nieman K, Cademartiri F, Lemos PA, Raaijmakers R, Pattynama PM, de Feyter PJ. Reliable noninvasive coronary angiography with fast submillimeter multislice spiral computed tomography. Circulation 2002;106: 2051–2054.
14. Pannu HK, Flohr TG, Corl FM, Fishman EK. Current concepts in multi–detector row CT evaluation of the coronary arteries: principles, techniques, and anatomy. Radiographics 2003;23:111–125.
15. Schoenhagen P, Halliburton SS, Stillman AE, et al. Noninvasive imaging of coronary arteries: current and future role of multi–detector row CT. Radiology 2004;232:7–17.
16. Schoepf UJ, Becker CR, Ohnesorge BM, Yucel EK. CT of coronary artery disease. Radiology 2004;232:18–37.

Bypass Graft Evaluation

17. Desjardins B, Kazerooni EA. ECG-gated cardiac CT. Am J Roentgenol 2004 Apr;182:993–1010.
18. Ha J, Cho S, Shim W, et al. Noninvasive evaluation of coronary artery bypass graft patency using three-dimensional angiography obtained with contrast-enhanced electron beam CT. Am J Roentgenol 1999;172:1055–1059.
19. Lu B, Dai RP, Jing BL, et al. Evaluation of coronary artery bypass graft patency using three-dimensional reconstruction and flow study on electron beam tomography. J Comput Assist Tomogr 2000;24:663–670.
20. Pannu HK, Flohr TG, Corl FM, Fishman EK. Current concepts in multi–detector row CT evaluation of the coronary arteries: principles, techniques, and anatomy. Radiographics 2003;23:111–125.
21. Ropers D, Ulzheimer S, Wenkel E, et al. Investigation of aortocoronary artery bypass grafts by multislice spiral computed tomography with electrocardiographic-gated image reconstruction. Am J Cardiol 2001;88: 792–795.
22. Schoepf UJ, Becker CR, Ohnesorge BM, Yucel EK. CT of coronary artery disease. Radiology 2004;232:18–37.
23. Willmann JK, Weishaupt D, Kobza R, Verdun FR, et al. Coronary artery bypass grafts: ECG-gated multi–detector row CT angiography—influence of image reconstruction interval on graft visibility. Radiology 2004;232: 568–577.

Aberrant Right Coronary Artery

24. Angelini P, Velasco JA, Flamm S. Coronary anomalies: incidence, pathophysiology, and clinical relevance. Circulation 2002;105:2449–2454.
25. Dirksen M, Bax J, Blom N, et al. Detection of malignant right coronary artery anomaly by multi-slice CT coronary angiography. Eur Radiol 2002;12:S177–S180.

26. McConnell MV, Ganz P, Selwyn AP. Identification of anomalous coronary arteries and their anatomic course by magnetic resonance coronary angiography. Circulation 1995 Dec;92(11):3158–3162.
27. Ropers D, Moshage W, Daniel WG. Visualization of coronary artery anomalies and their anatomic course by contrast-enhanced electron beam tomography and three-dimensional reconstruction. Am J Cardiol 2001 Jan;87(2):193–197.
28. Ropers D, Gehling G, Pohle K, et al. Anomalous course of the left main or left anterior descending coronary artery originating from the right sinus of valsalva: identification of four common variations by electron beam tomography. Circulation 2002;105:e42–e43.

Pulmonary Vein Evaluation

29. Cronin P, Sneider MB, Kazerooni EA, et al. MDCT of the left atrium and pulmonary veins in planning radiofrequency ablation for atrial fibrillation: a how-to guide. Am J Roentgenol 2004 Sep;183:767–778.
30. Lacomis JM, Wigginton W, et al. Multi–detector row CT of the left atrium and pulmonary veins before radio-frequency catheter ablation for atrial fibrillation. Radiographics 2003;23:S35–S48.
31. Lin WS, Prakash VS, Tai CT, et al. Pulmonary vein morphology in patients with paroxysmal atrial fibrillation initiated by ectopic beats originating from the pulmonary veins: implications for catheter ablation. Circulation 2000;101:1274–1281.
32. Scharf C, Sneider M, Case I, et al. Anatomy of the pulmonary veins in patients with atrial fibrillation and effects of segmental ostial ablation analyzed by computed tomography. J Cardiovasc Electrophysiol 2003;14: 150–155.
33. Yang M, Akbari H, Redd GP, Higgins CB. Identification of pulmonary vein stenosis after radiofrequency ablation for atrial fibrillation using MRI. J Comput Assist Tomogr 2001;25:34–35.

Atrial Myxoma

34. Burke AP, Virmani R. Cardiac myxoma: a clinicopathologic study. Am J Clin Pathol 1993;100:671–680.
35. Grebenc ML, Rosado-de-Christenson ML, Green CE, Burke AP, Galvin JR. From the archives of the AFIP: cardiac myxoma: imaging features in 83 patients. Radiographics 2002;22:673–689.
36. Gotway MB, Nagai BK, Reddy GP, Patel RA, Higgins CB, Webb WR. Incidentally detected cardiovascular abnormalities on helical CT pulmonary angiography: spectrum of findings. Am J Roentgenol 2001 Feb;176:421–427.
37. Reynen K. Cardiac myxomas. N Engl J Med 1995;333:1610–1617.

Coronary Stent Evaluation

38. Funabashi N, Komiyama N, Komuro I. Patency of coronary artery lumen surrounded by metallic stent evaluated by three dimensional volume rendering images using ECG gated multislice computed tomography. Heart 2003;89:388.
39. Hong C, Chrysant GS, Woodard PK, Bae KT. Coronary artery stent patency assessed with in-stent contrast enhancement measured at multi-detector row CT angiography: initial experience. Radiology 2004 Oct;233(1): 286–291.

40. Maintz D, Juergens KU, Wichter T, Grude M, Heindel W, Fischbach R. Imaging of coronary artery stents using multislice computed tomography: in vitro evaluation. Eur Radiol 2003;13:830–835.
41. Maintz D, Grude M, Fallenberg EM, Heindel W, Fischbach R. Assessment of coronary arterial stents by multislice-CT angiography. Acta Radiol 2003 Nov;44(6):597–603.
42. Nieman K, Cademartiri F, Raaijmakers R, Pattynama P, De Feyter P. Non-invasive angiographic evaluation of coronary stents with multi-slice spiral computed tomography. Herz 2003;28:136–142.
43. Pump H, Mohlenkamp S, Sehnert CA, et al. Coronary arterial stent patency: assessment with electron-beam CT. Radiology 2000;214:447–452.